Energy transfer processes in Yb^{3+}–Tm^{3+} co-doped sodium alumino-phosphate glasses with improved 1.8 μm emission

2008 J. Phys.: Condens. Matter 20 255240

(http://iopscience.iop.org/0953-8984/20/25/255240)

J. Phys.: Condens. Matter **20** (2008) 255240 (6pp) doi:10.1088/0953-8984/20/25/255240

Energy transfer processes in Yb^{3+}–Tm^{3+} co-doped sodium alumino-phosphate glasses with improved 1.8 μm emission

Andrea S S de Camargo[1], Idelma A A Terra, Luiz Antonio de O Nunes and M Siu Li

Instituto de Física de São Carlos, Universidade de São Paulo, 13560-970, São Carlos—SP, Brazil

E-mail: andreasc@ifsc.usp.br

Received 29 February 2008, in final form 21 April 2008
Published 22 May 2008
Online at stacks.iop.org/JPhysCM/20/255240

Abstract

Sodium alumino-phosphate glasses co-doped with Yb^{3+} and Tm^{3+} ions have been prepared with notably low OH^- content, and characterized from the viewpoint of their spectroscopic properties. In these glasses, Yb^{3+} acts as an efficient sensitizer of excitation energy at 0.98 μm—which can be provided by high power and low cost diode lasers, and subsequently undergoes non-resonant energy transfer to Tm^{3+} ions ($^2F_{5/2}$, $^3H_6 \rightarrow {}^2F_{7/2}$, $^3H_5$). Through this process, the emitting level $^3F_4$ is rapidly populated, generating improved emission at 1.8 μm ($^3F_4 \rightarrow {}^3H_6$). In order to guarantee the efficiency of such favorable energy transfer, energy losses via multiphonon decay, Yb–Yb radiative trapping, and non-radiative transfer to OH^- groups were evaluated, and minimized when possible. The dipole–dipole energy transfer microscopic parameters corresponding to $Yb^{3+} \rightarrow Tm^{3+}$, $Yb^{3+} \rightarrow Yb^{3+}$ and $Tm^{3+} \rightarrow Tm^{3+}$ transfers, calculated by the Förster–Dexter model, are $C_{Yb-Tm} = 2.9 \times 10^{-40}$ cm^6 s^{-1}, $C_{Yb-Yb} = 42 \times 10^{-40}$ cm^6 s^{-1} and $C_{Tm-Tm} = 43 \times 10^{-40}$ cm^6 s^{-1}, respectively.

1. Introduction

Ever since the contributions made by Auzel [1] on the energy transfer processes involving sensitizer and activator ions, it has been largely recognized that an appropriate combination of ionic species and concentrations can lead to the improvement of rare earth ion (RE^{3+}) doped laser material efficiencies. Among the most employed sensitizers, Yb^{3+} is the most advantageous one, presenting only two energy levels in the $4f^{13}$ configuration (the ground state $^2F_{7/2}$ and the excited state $^2F_{5/2}$), separated by 10 000 cm^{-1}. This peculiar energy level configuration allows excitation with high power 0.98 μm commercial diode lasers, high energy storage capability at the metastable level $^2F_{5/2}$, low heat generation, and, most important, the absence of excited state absorptions [2–4]. Thus, Yb^{3+} can be efficiently used in generating broadband emission at around 1.0 μm (including amplification of femtosecond pulses), and to improve the intensity of near-infrared and/or upconversion emissions of other rare earth ions like Tm^{3+}, with emissions at 1.8 μm and in the blue spectral region [5, 6]. It is worth noting that when it comes to diode excitation in the near-infrared, thulium ions themselves do not absorb at 0.98 μm, and present very low absorption at 0.8 μm, thus the Yb^{3+}–Tm^{3+} co-doping scheme is much preferred.

Because of advantageous properties such as better thermal and thermo-optical properties and lower optical dispersion than other laser glasses, RE^{3+} doped phosphate glasses have been pursued as promising for high power laser applications [4, 7]. One disadvantage of these glasses, however, is that they are hygroscopic and the presence of OH^- groups, acting like high energy phonons, can seriously affect the fluorescence quantum efficiency of the emitting RE^{3+}. The main sources of OH^- groups are the starting materials and atmospheric moisture during the melt; therefore, there are means to reduce its incorporation in the glass, by variations in composition and synthesis procedures. For instance, reduction of OH^- absorption bands has been reported for glasses in which dry-air bubbling was done through the melt [8, 9], and also it is well known that the addition of aluminum oxide improves

[1] Author to whom any correspondence should be addressed.

the chemical stability of metaphosphate glasses [10, 11]. Recently, Yb^{3+} and Yb^{3+}–Tm^{3+} doped sodium alumino-phosphate glasses, nearly free from OH^-, have been prepared under N_2 atmosphere, and characterized from the viewpoint of optical spectroscopy [3, 4, 6]. For Yb^{3+}–Tm^{3+} co-doped samples, we have verified that a set of samples prepared in air presents a significantly lower fluorescence quantum efficiency of Tm^{3+} near-infrared and visible levels in comparison to samples prepared in N_2 [6]. Still, to be able to further evaluate the effectiveness of Yb^{3+}–Tm^{3+} co-doping in improving Tm^{3+}1.8 μm emission, a more detailed quantitative study of $Yb^{3+} \rightarrow Tm^{3+}$ transfer is desirable.

In this work we present a detailed characterization of two sets of sodium alumino-phosphate samples doped with 5 wt% Yb_2O_3 and various Tm_2O_3 concentrations (0.1–2.0 wt% Tm_2O_3), prepared in air and N_2 atmospheres. The $Yb^{3+} \rightarrow Tm^{3+}$ energy transfer, as well as the $Yb^{3+} \rightarrow Yb^{3+}$ and $Tm^{3+} \rightarrow Tm^{3+}$ energy migrations, are evaluated in terms of the microscopic energy transfer parameters C_{DA} (donor–acceptor transfer) and C_{DD} (donor–donor) [12–15]. Additionally, the effects of multiphonon decay, radiation trapping in Yb^{3+}, and energy transfer from the RE^{3+} to the OH^- ions are also approached.

2. Experimental details

Two sets of sodium alumino-phosphate glasses with nominal composition $(1-x)[57(NaPO_3)_3 + 38Al(PO_3)_3] + 5Yb_2O_3 + xTm_2O_3$, where $x = 0.1$, 0.5, 1.0, 1.5 and 2.0 wt%, were prepared in either air or N_2 atmosphere. In the first case, the precursors were weighed and melted at 1100 °C, for 30 min, and the melts were cast in a brass mold pre-heated to 250 °C. For the set prepared in N_2 atmosphere, the furnace was placed inside a sealed camera, where vacuum was made first, followed by N_2 injection, and the same heating and quenching procedures were carried out. In order to reduce mechanical stress, all the samples were subjected to a second heat treatment at 350 °C for 6 h and slowly cooled to room temperature. The high optical quality glass samples were cut and polished.

The spectroscopic measurements were all made at room temperature. Undoped samples, with 0.8 mm thickness, were characterized by FT-IR up to 5.5 μm (1820 cm^{-1}), using a Nicolet Magna IR 850 spectrophotometer. The near-infrared to visible absorption spectra (0.35–2.0 μm) were measured in a Perkin Elmer model Lambda 900 spectrophotometer. The emission spectra of thulium and ytterbium ions were obtained using as excitation source either an Ar^+ laser at 0.514 μm or a diode laser at 0.98 μm. The luminescent signals were dispersed by a single (0.3 m) monochromator, detected by an InGaAs detector model EG&G HTE2642 (1.0 μm emission) or an InAs detector model EG&G J12D (1.8 μm), and amplified by a lock-in. All the samples had the same size and thickness, and were carefully measured in the same position, in order to allow the comparison of their integrated intensities. Excited state lifetime values were obtained from transient luminescence curves, which were measured by exciting the samples with a Nd:YAG pumped optical parametric oscillator (Continuum Surelite SLII-10), using the same monochromator, the InAs detector or a photomultiplier, and a digital oscilloscope (Tektronix TDS380).

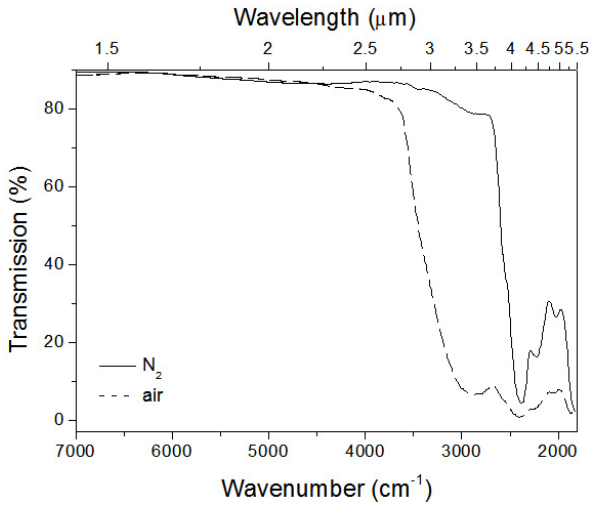

Figure 1. Infrared transmission spectra of undoped 0.8 mm thick sodium alumino-phosphate glasses, obtained in N_2 (solid line) and air (dashed line) atmospheres.

3. Results and discussion

The transmission spectra of 0.8 mm thick undoped glass samples obtained in air (dashed line) and nitrogen (solid line) atmospheres are presented in figure 1. It is clearly noted that the choice of an oxygen free atmosphere for the synthesis led to a significant decrease of the OH^- group absorption in the range 2700–3700 cm^{-1}. While both samples present a transmission of ~87% up to 1.4 μm, the transmission window of the sample prepared in N_2 is about 30% more extensive (up to 3.7 μm) than that of the one prepared in air. The absorption coefficient α_{OH} at 3000 cm^{-1} is often used as a measurement of the OH^- concentration and OH^- content in the samples, according to [9, 16]

$$\alpha_{OH} = \log(T_0/T_D)/d; \qquad OH^- \text{content(ppm)} = 30\alpha_{OH}, \tag{1}$$

where T_0 is the highest transmission, usually at around 7000 cm^{-1}, T_D is the transmission at 3000 cm^{-1}, and d is the thickness of the sample. The α_{OH} values are 12.7 and 0.44 cm^{-1} for samples obtained in air and N_2, respectively, and the OH^- contents are 381 and 13.2 ppm. Both Yb^{3+} and Tm^{3+} emissions at 1.0 and 1.8 μm, respectively, can be negatively affected by non-radiative energy transfer to OH^- groups, because their corresponding wavenumbers (10 000 and 5555 cm^{-1}, respectively) fall within the range of broad overtone bands corresponding to O–H stretching vibrations. In this sense, it has been suggested that the energy transfer rate to OH^- groups can be written as a function of a constant k_{OH} related to the extent of interaction between the rare earth and OH^- ions, independently from the concentration of either RE^{3+} or OH^- [9, 17]. But, because we cannot determine the distribution and bond lengths of RE^{3+} and OH^- ions in the

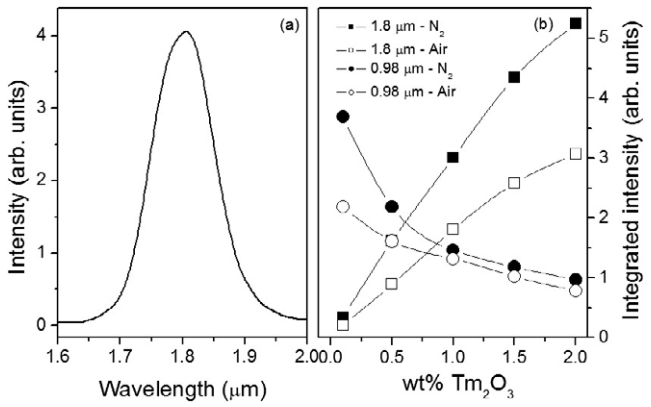

Figure 2. (a) Emission spectrum of a 5Yb–2Tm sodium alumino-phosphate glass ($^3F_4 \rightarrow {}^3H_6$ transition); (b) integrated emission intensities of Yb^{3+} (1.0 μm) and Tm^{3+} (1.8 μm) for samples obtained in air (open symbols) and N_2 (solid symbols) atmospheres, as a function of Tm_2O_3 concentration. In (b), the scale should only serve for comparison of tendencies as a function of atmosphere and Tm^{3+} concentration, whereas intensities of different emissions, for the same doping level, should not be compared.

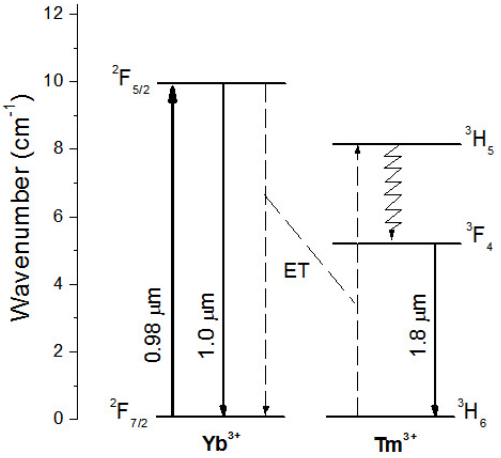

Figure 3. Partial energy level scheme of Yb^{3+} and Tm^{3+} ions. The solid lines indicate the 0.98 μm excitation and the emissions at 1.0 and 1.8 μm, and the dashed lines correspond to the $Yb^{3+} \rightarrow Tm^{3+}$ energy transfer (ET).

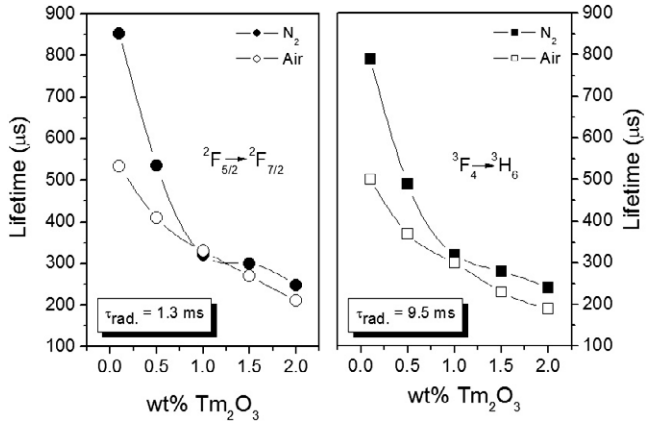

Figure 4. Lifetime values of sodium alumino-phosphate glasses obtained in N_2 (closed symbols), and air (open symbols) atmospheres: (a) ytterbium $^2F_{5/2} \rightarrow {}^2F_{7/2}$ transition at 1.0 μm; (b) thulium $^3F_4 \rightarrow {}^3H_6$ transition at 1.8 μm. The values were obtained from the emission intensity decay curves in time, and the calculated radiative lifetime values are shown for comparison.

studied samples, any attempt to quantify the transfer rate would be far from ideal. Still, it can be expected that the Yb^{3+}–Tm^{3+} co-doped samples prepared in N_2 (with much lower OH^- content) present lower probability of $RE^{3+} \rightarrow OH^-$ energy transfer than those samples prepared in air.

As for the $Yb^{3+} \rightarrow Tm^{3+}$ energy transfer, more substantiated conclusions can be drawn. Figure 2(a) presents the representative Tm^{3+} emission spectrum of a sample doped with 5 wt% Yb_2O_3–2 wt% Tm_2O_3 (5Yb–2Tm). Figure 2(b) presents the evolution curves of integrated emission intensities of Tm^{3+} (1.8 μm—squares) and Yb^{3+} (1.0 μm—circles), for the sets of samples obtained in air (open symbols) and in N_2 (solid symbols), as a function of Tm^{3+} concentration. According to the partial energy levels diagram in figure 3, it is seen that for both sets of samples subjected to 0.98 μm excitation there is a progressive increase of 1.8 μm emission intensity, with increasing Tm^{3+} concentration. This intensity increase is directly accompanied by a decrease of Yb^{3+} 1.0 μm emission intensity, giving clear evidence of $Yb^{3+} \rightarrow Tm^{3+}$ non-radiative energy transfer ($^2F_{5/2}$, $^3H_6 \rightarrow {}^2F_{7/2}$, $^3H_5$). Once level $^3H_5$ is excited, the emitting level $^3F_4$, that lies at about 2700 cm^{-1} below it, is efficiently pumped by multiphonon decay. Because the concentration of Yb^{3+} is high and constant in all the samples (5 wt% Yb_2O_3), the energy transfer is favored by Yb^{3+}–Yb^{3+} energy migration, ($^2F_{5/2}$, $^2F_{7/2} \rightarrow {}^2F_{7/2}$, $^2F_{5/2}$), as well as by Tm^{3+}–Tm^{3+} migration ($^3H_6$, $^3F_4 \rightarrow {}^3F_4$, $^3H_6$), with increasing Tm^{3+} concentration. Through these energy migrations, the excitation energy is spread among the activator ions, but the transfer to OH^- groups is also favored. If comparison is made between the curves of Yb^{3+} emission in figure 2(b), it is clear that for the sample with very low Tm^{3+} concentration (0.1%)—where mainly Yb^{3+}–Yb^{3+} migration is present, the sample made in air presents a 40% lower intensity than the one made in N_2. However, as the Tm^{3+} concentration is increased (and that of Yb^{3+} is kept constant), the $Yb^{3+} \rightarrow OH^-$ transfer reaches saturation, and the $Yb^{3+} \rightarrow Tm^{3+}$ transfer is largely favored. In the same way, for the 1.8 μm emission intensities of 5Yb–0.1Tm samples, little difference is observed between samples made in air and N_2, because the Tm^{3+} migration followed by transfer to OH^- is less probable. However, for higher Tm^{3+} concentrations the intensity differences increase, up to the 40% figure in samples doped with 2.0 wt% Tm_2O_3.

The results of lifetime measurements (figure 4) corroborate this discussion. The calculated radiative lifetime (τ_{rad}) values of Yb^{3+} and Tm^{3+} in the sodium alumino-phosphate glass matrix are 1.3 and 9.5 ms respectively. Since the Yb^{3+} levels are separated by ~10 000 cm^{-1} and the phonon energy of this glass is 1200 cm^{-1}, it has been verified that samples prepared in N_2, singly doped with up to 0.5 wt% Yb_2O_3 (0.5Yb), present a lifetime value very similar to the calculated one, leading to $\eta \approx 1$ [3]. This is an indication of negligible OH^- content in these samples, which were prepared by the same

methodology as used in the present work. Furthermore, within the set of samples prepared in N_2, it is seen in figure 4(a) that the lifetime value of Yb^{3+} level $^2F_{5/2}$ for the sample 5Yb–0.1Tm is 850 μs, in agreement with the result presented in [3] for a 5Yb sample. As to be expected, with increasing Tm^{3+} concentration, the $Yb^{3+} \rightarrow Tm^{3+}$ energy transfer acts like an additional depopulation channel to level $^2F_{5/2}$, and a decrease in its lifetime value is observed for both sets of samples. For the emitting level $^3F_4$ (figure 4(b)), a maximum $\eta \approx 0.08$ is obtained from the τ_{exp}/τ_{rad} ratio [6]. The reason for this low value is intrinsic to the $^3F_4 \rightarrow {}^3H_6$ transition in high phonon energy glasses, because the small energy gap (5555 cm^{-1}) can be bridged by some four to five phonons. Once again, it is observed that as the Tm^{3+} concentration is increased an accompanying decrease in lifetime values is observed, due to activation of the Tm–Tm energy migration followed by transfer to OH^- or other defects. By comparison of the curves corresponding to the sets of samples prepared in air and N_2 (figures 4(a) and (b)), it is verified that, similarly to the behavior of luminescence intensities (figure 2), the $RE^{3+} \rightarrow OH^-$ transfer effect, related to a decrease in lifetime values, is more pronounced for the 5Yb–0.1Tm samples. When the $Yb^{3+} \rightarrow Tm^{3+}$ transfer starts playing a role, it competes with the $RE^{3+} \rightarrow OH^-$ transfer.

As previously pointed out, it is not possible to accurately determine these energy transfer rates without knowledge of the statistical distribution and RE^{3+}–RE^{3+} distances in the glass matrix. Yet, the microscopic energy transfer parameters C_{DA} (C_{DD}), which are directly proportional to the energy transfer probability P_{DA} (P_{DD}), can be obtained independently from RE^{3+} concentrations. In these parameters, the subscript DA denotes donor–acceptor transfer (as in the case of $Yb^{3+} \rightarrow Tm^{3+}$), and DD denotes donor–donor transfer (as in the case of RE^{3+} migrations). The energy transfer microparameters are frequently calculated using the Förster–Dexter model of multipolar interactions [12, 13], based on the spectral overlap of the donor ion emission with the acceptor (donor) ion absorption. For the most probable dipole–dipole resonant energy transfer mechanism the expression is [12]

$$C_{DA} = \frac{3\hbar^4 c^4 Q_A}{4\pi n^4 \tau_D} \int \frac{f_D(E) f_A(E)}{E^4} \, dE, \qquad (2)$$

where $\hbar$ is the Planck's constant, c is the speed of light, Q_A is the normalized acceptor ion absorption cross section, n is the glass refractive index, τ_D is the donor ion radiative lifetime value, and the integral corresponds to the spectral overlap of donor ion emission and acceptor ion absorption, as a function of energy E. The dipole–dipole energy transfer probability is then given by $P_{DA} = C_{DA}/R^6 (s^{-1})$, where R is the average ion–ion distance.

In order to calculate the overlap integrals in equation (2), the absorption cross section (σ_{abs}) and emission cross section (σ_{emis}) spectra of Yb^{3+} and Tm^{3+} need to be carefully obtained. The former is directly calculated from the experimental absorption coefficients α (cm^{-1}) and the ionic density N (cm^{-3}), according to $\sigma_{abs}(\lambda) = \alpha(\lambda)/N$. The latter cannot be obtained directly, but it can be calculated from the σ_{abs} spectrum, using the reciprocity method [18]:

$$\sigma_{emis}(\lambda) = \sigma_{abs}(\lambda) \frac{Z_l}{Z_u} \exp\left(\frac{E_{zl} - hc\lambda^{-1}}{kT}\right), \qquad (3)$$

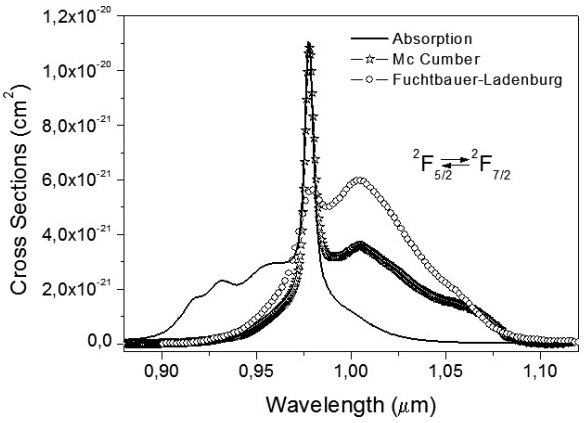

Figure 5. Comparison of the stimulated emission cross section spectra scaled using the radiative lifetime value in the Fuchtbauer–Ladenburg expression (open circles) and the McCumber theory (open stars) with the ground state absorption cross section spectrum.

where Z_l and Z_u are the partition functions of lower and upper levels respectively, k is the Boltzmann constant, T is the temperature in Kelvin, and E_{zl} is the zero-line energy, defined as the energy separation between the lowest components of the upper and lower states. As a means to compare the spectrum lineshape resulting from equation (3) with the one obtained experimentally, with 0.98 μm excitation, the emission cross section spectra were also obtained using the well know Fuchtbauer–Ladenburg (FL) expression [19],

$$\sigma_{emis}(\lambda) = \frac{\lambda^4}{8\pi c n^2 \tau} \frac{I(\lambda)}{\int I(\lambda) d\lambda}, \qquad (4)$$

where τ is the emitting ion radiative lifetime value and the second term in the expression is the normalized emission intensity lineshape function. For the case of non-resonant energy transfer, as in the case of $Yb^{3+} \rightarrow Tm^{3+}$, the spectral overlap can be achieved by the creation (Stokes) or annihilation (anti-Stokes) of high energy phonons in the matrix. This procedure, which was used in this work, is based on the formalism proposed by Miyakawa and Dexter [14] and further developed by Tarelho *et al* [15].

The emission cross section spectra of Yb^{3+} ($^2F_{5/2} \rightarrow {}^2F_{7/2}$), obtained by these two methods, are presented in figure 5, along with the absorption cross section spectrum. As clearly noticed, the intensity scales of both emission spectra do not coincide. The intense peak at 0.978 μm is not observed for the FL spectrum, due to an appreciable radiation trapping effect. This effect is due to a continuous process in which spontaneously emitted photons are trapped by reabsorption by ions in the ground state, leading to variations in the spectral lineshapes, and a net increase of the fluorescence lifetime measured over the volume of the sample, when compared to the lifetime of a single isolated ion [20, 21]. It is well known to happen in Yb^{3+} doped materials, because of the two level 4f configuration of this ion. The probability of radiation trapping increases with increasing Yb^{3+} concentration [21], and thus it is advised that thin samples, or frontal excitation of samples, be used for the characterization by luminescence measurements.

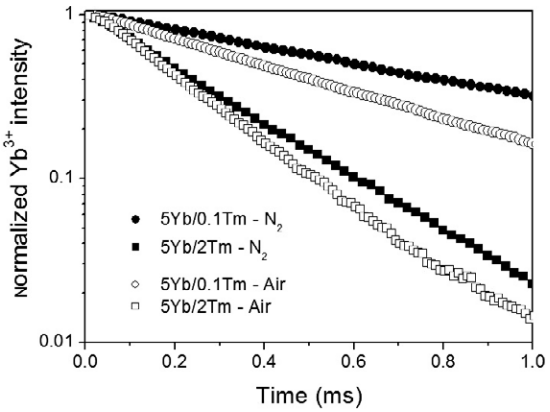

Figure 6. Transient Yb^{3+} emission (1.0 μm) for sodium alumino-phosphate glass samples 5Yb–0.1Tm and 5Yb–2Tm, obtained in N_2 (solid symbols) and air (open symbols).

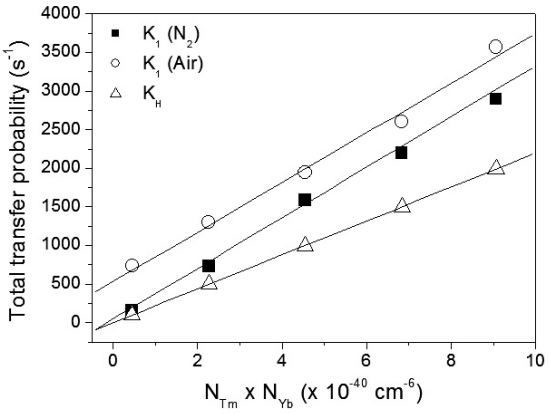

Figure 7. Dependence of total energy transfer ($Yb^{3+} \rightarrow Tm^{3+}$ and $Yb^{3+} \rightarrow OH^-$) probability factors K_1, and the factor K_H, on the product of ionic concentrations.

Table 1. Energy transfer microscopic parameters obtained using the dipole–dipole interaction expression (equation (2)) of the Förster–Dexter model.

	C_{Yb-Tm}	C_{Yb-Yb}	C_{Tm-Tm}
Parameters ($cm^6\ s^{-1}$)	2.9×10^{-40}	42×10^{-40}	43×10^{-40}

In fact, the effect is clearly noticed on the FL spectrum in figure 5 because the luminescence measurements were made with diode laser excitation through the volume of the sample (lateral excitation). In contrast, the lifetime values presented in figure 4 were derived from measurements made with frontal excitation with the OPO laser, and thus the effect of radiation trapping is minimized in the transients. Proof of this is given by the agreement of the lifetime values of the sample 5Yb–0.1Tm with that of a 5Yb sample, prepared under the same conditions, in which the effect was assured not to be present [3]. Even if radiation trapping played a role in these co-doped samples, it would be a favorable one, because a longer lifetime value of $^2F_{5/2}$ would actually favor the $Yb^{3+} \rightarrow Tm^{3+}$ energy transfer, inclusively by increasing Yb^{3+} migration. In obtaining the energy transfer microscopic parameters presented in table 1, it was verified that the use of either the FL or the McCumber spectra in figure 5 leads to values within the errors involved in the calculations.

From the analysis of the values presented in table 1, it can be understood that, for the same levels of ionic concentrations and distributions, the energy migrations among Yb^{3+} ions (C_{Yb-Yb}), and among Tm^{3+} ions (C_{Tm-Tm}), are much more probable than the $Yb^{3+} \rightarrow Tm^{3+}$ energy transfer (C_{Yb-Tm}). This is also the case for other Yb^{3+}–Tm^{3+} co-doped materials like KY_3F_{10}, $LiYF_4$, $YAlO_3$ and YVO_4 crystals [2, 15, 22]. This result is to be expected because, since the migrations are resonant processes, the overlap integrals in equation (2) have much larger values than that for the case of non-resonant $Yb^{3+} \rightarrow Tm^{3+}$ transfer, which has to be phonon aided.

Since the early works of Yokota and Tanimoto [23] and Burshtein [24], it is known that the migration assisted energy transfer significantly increases the probability of interaction between sensitizer and activator ions of different species. The typical characteristic of migration assisted energy transfer, which is an exponential decay mode, can be identified in the transient emission curves of Yb^{3+} in co-doped samples, as presented in figure 6. According to Braud *et al* [2], if the migration assisted energy transfer dominates over the direct sensitizer–activator transfers, as has proven to be the case in this work, an energy transfer probability K_1 (s^{-1}) is found to be time independent, and can be related to the experimental lifetimes by

$$K_1 = \frac{1}{\tau(^2F_{5/2})_{Yb-Tm}} - \frac{1}{\tau(^2F_{5/2})_{Yb}}. \qquad (5)$$

The expression for K_1 only takes into account the $Yb^{3+} \rightarrow Tm^{3+}$ transfer probability and not that of $Yb^{3+} \rightarrow OH^-$, which might constitute an additional loss channel for Yb^{3+} $^2F_{5/2}$ population. Still, in order to evaluate the dependence of K_1 with the ionic densities of Yb^{3+} and Tm^{3+} ions, plots of K_1 versus the product $N_{Tm} \times N_{Yb}$ for both sets of samples, prepared in N_2 (solid squares), and air (open circles), are presented in figure 7. These plots, which in truth represent the total energy transfer probabilities from Yb^{3+}, can be viewed as depopulation mechanisms of level $^2F_{5/2}$. In agreement with [2] it can be seen that in the range of concentrations used in this work $K_1 = N_{Tm}N_{Yb}\alpha_1$, where α_1 is a constant approximately equal to 3.2×10^{-38} for both K_1 plots. Despite nearly equal inclinations, it is seen that the K_1 plot corresponding to the set of samples prepared in air presents a nearly constant increase in transfer probabilities in relation to the one corresponding to the set of samples prepared in N_2. Since the RE^{3+} concentrations are the same in both sets, such an increase can only be attributed to the $RE^{3+} \rightarrow OH^-$ transfer, more pronounced in air-prepared samples. This process is likely to be favored by increasing Tm^{3+} concentrations because the energy migration through the $^3F_4$ level favors energy spreading through the samples, and thus transfer to OH^-.

In the Burshtein model (hoping model) applicable to the case when the probability of energy migration among Yb sensitizers is higher than the probability of direct $Yb^{3+} \rightarrow Tm^{3+}$ energy transfer, $K_1 = K_H$, and the transfer probability

K_H can be written as a function of the previously calculated microscopic parameters as

$$K_H = [\pi(2\pi/3)^{5/2} C^{1/2}_{\mathrm{Yb-Tm}} C^{1/2}_{\mathrm{Yb-Yb}}] N_{\mathrm{Tm}} N_{\mathrm{Yb}}. \quad (6)$$

Note that, similarly to the K_1 factor, K_H also does not take into account $Yb^{3+} \rightarrow OH^-$ transfer. Its values are plotted in figure 7 ($\alpha_1 = 2.2 \times 10^{-38}$), as a function of ionic densities, for comparison with the K_1 plots. The discrepancy between inclinations of K_1 and K_H plots can be due to two reasons: (i) inaccuracy in the determination of $C_{\mathrm{Yb-Tm}}$ and $C_{\mathrm{Yb-Yb}}$ microscopic parameters used to obtain K_H; (ii) additional contribution of $Yb^{3+} \rightarrow OH^-$ transfer, that influences K_1, even in the samples prepared in N_2. Both hypotheses are plausible if one considers that, due to non-resonance of donor ($^2F_{5/2}$) emission and acceptor ($^3H_5$) absorption, there are errors involved mostly in the calculation of $C_{\mathrm{Yb-Tm}}$, and, as previously seen, the OH^- content in samples prepared in N_2 is low, but not zero.

In figure 7 it is seen that for a 5Yb–0.1Tm sample prepared in N_2, for which the Tm^{3+} energy migration is less probable, the probabilities K_1 and K_H are practically the same because the $Yb^{3+} \rightarrow OH^-$ transfer is much less probable. For samples with higher Tm^{3+} content, though, the K_1 values are higher than K_H, in part because the higher Tm^{3+} migration favors transfer to OH^-, but mostly because it favors $Yb^{3+} \rightarrow Tm^{3+}$ transfer. Based on the OH^- contents calculated according to equation (1), the number of OH^- ions distributed in the volume of the glasses prepared in air was calculated to be 3.4×10^{19} cm^{-3}, while that of glasses prepared in N_2 is 0.12×10^{19} cm^{-3}. The latter is much lower and the former is only comparable to that of Tm^{3+} ions in samples doped with up to 0.5 wt% Tm_2O_3 (4.75×10^{19} Tm^{3+} ions cm^{-3}), whereas the number of Yb^{3+} ions is always much higher (4.77×10^{20} Yb^{3+} ions cm^{-3}). This means that, if, as expected, there is a statistical distribution of OH^- and Tm^{3+} ions, the $Yb^{3+} \rightarrow OH^-$ energy transfer is only significantly competitive with that of $Yb^{3+} \rightarrow Tm^{3+}$ for low Tm^{3+} doped samples (up to 0.5 wt%). It should also be noted that, since in the expression for the K_H plot the Tm^{3+} energy migration is not taken into account, this could explain, in part, the deviation from the K_1 plot for samples prepared in N_2. Unfortunately, to the best of our knowledge there are no reports in the literature for the $C_{\mathrm{Yb-Tm}}$ parameter in phosphate glasses, that would enable us to compare the errors involved in calculation. However, we believe that, considering the proposed models, an agreement of order of magnitude in $C_{\mathrm{Yb-Tm}}$ is very satisfactory.

4. Conclusions

Sodium alumino-phosphate glasses co-doped with Yb^{3+} and Tm^{3+} prepared under controlled N_2 atmosphere were obtained with much lower OH^- content than samples, with the same composition, prepared in air. The $Yb^{3+} \rightarrow Tm^{3+}$ energy transfer process was shown to be effective in increasing the 1.8 μm emission of the latter, which is also favored by the resonant Yb^{3+}–Yb^{3+} and Tm^{3+}–Tm^{3+} energy migrations over levels $^2F_{5/2}$ and $^3F_4$ respectively. Although the energy migrations can also favor energy transfer from the rare earth ions to OH^- groups, it was verified that this process would only be of significant relevance, in terms of competition with $Yb^{3+} \rightarrow Tm^{3+}$, for samples doped with low concentration of Tm^{3+}. Furthermore, it was verified that the effect of radiation trapping in Yb^{3+} ions is only an issue for thick samples, and under volumetric excitation. Since this is the case in a typical solid state laser cavity, radiation trapping can actually be viewed as favorable for Tm^{3+} emissions, since induction of a longer lifetime for $^2F_{5/2}$ would, in principle, favor energy migration and $Yb^{3+} \rightarrow Tm^{3+}$ transfer.

Acknowledgments

The authors would like to thank Professor Hellmut Eckert for the valuable discussions, and the Brazilian agencies FAPESP—*Fundação de Amparo à Pesquisa de São Paulo*— and CNPq—*Conselho Nacional de Desenvolvimento Científico e Tecnológico*—for the financial support.

References

[1] Auzel F E 1973 *Proc. IEEE* **61** 758
[2] Braud A, Girard S, Doualan J L, Thuau M, Moncorgé R and Tkachuk A M 2000 *Phys. Rev.* B **61** 5280
[3] Quirino W G, Bell M J V, Oliveira S L and Nunes L A O 2005 *J. Non-Cryst. Solids* **351** 2042
[4] Jacinto C, Oliveira S L, Nunes L A O, Catunda T and Bell M J V 2005 *Appl. Phys. Lett.* **86** 071911 and references therein
[5] Diening A, Möbert P E-A and Huber G 1998 *J. Appl. Phys.* **84** 5900
[6] Terra I A A, de Camargo A S S, Nunes L A O, Carvalho R A and Li M S 2006 *J. Appl. Phys.* **100** 123103
[7] Paoloni S, Hein J, Töpfer T, Walther H G, Sauerbrey R, Ehrt D and Wintzer W 2004 *Appl. Phys.* B **78** 415 and references therein
[8] Kobayashi K 1997 *J. Eur. Ceram. Soc.* **17** 49
[9] Zhang L and Hu H 2001 *J. Non-Cryst. Solids* **292** 108
Zhang L and Hu H 2002 *J. Phys. Chem. Solids* **63** 575
[10] Liu H S, Shih P Y and Chin T S 1996 *Phys. Chem. Glasses* **37** 227
[11] Minami T and Mackenzie D 1977 *J. Am. Ceram. Soc.* **60** 232
[12] Dexter D L 1953 *J. Chem. Phys.* **21** 836
[13] Förster V T 1948 *Ann. Phys.* **2** 55
[14] Miyakawa T and Dexter D L 1970 *Phys. Rev.* B **1** 2961
[15] Tarelho L V G, Gomes L and Ranieri I M 1997 *Phys. Rev.* B **56** 14344
[16] Ebendorff-Heidepriem H, Seeber W and Ehrt D 1993 *J. Non Cryst. Solids* **163** 74
[17] Stokowski S E and Krashkevich D 1986 *Mater. Res. Soc. Symp. Proc.* **61** 273
[18] McCumber D E 1964 *Phys. Rev.* **136** A954
[19] Miniscalco W J and Quimby R S 1991 *Opt. Lett.* **16** 258
[20] Sumida D S and Fan T Y 1994 *Opt. Lett.* **19** 1343
[21] Dai S, Yang J, Wen L, Hu L and Jiang Z 2003 *J. Lumin.* **104** 55
[22] Mita Y, Togashi M, Umetsu Y and Yamamoto H 2001 *Japan. J. Appl. Phys.* **40** 5925
[23] Yokota M and Tanimoto O 1967 *J. Phys. Soc. Japan* **22** 779
[24] Burshtein A I 1972 *Zh. Eksp. Teor. Phys.* **62** 1695
Burshtein A I 1972 *Sov. Phys.—JETP* **35** 882